POLITECNICO DI TORINO
Repository ISTITUZIONALE

Comparison of the Tribological Behaviour of Various Graphene Nano-Coatings as a Solid Lubricant for Copper

Original
Comparison of the Tribological Behaviour of Various Graphene Nano-Coatings as a Solid Lubricant for Copper / Goti, E., Mura, A., Wang, H., Ji, X., Kong, J.. - In: APPLIED SCIENCES. - ISSN 2076-3417. - 13:14(2023). [10.3390/app13148540]

Availability:
This version is available at: 11583/2980775 since: 2023-07-29T09:01:04Z

Publisher:
MDPI

Published
DOI:10.3390/app13148540

Terms of use:

This article is made available under terms and conditions as specified in the corresponding bibliographic description in the repository

Publisher copyright

(Article begins on next page)

19 November 2026

applied sciences

MDPI

Article

Comparison of the Tribological Behaviour of Various Graphene Nano-Coatings as a Solid Lubricant for Copper

Edoardo Goti [1], Andrea Mura [1,*], Haozhe Wang [2], Xiang Ji [2] and Jing Kong [2]

[1] Department of Mechanical and Aerospace Engineering, Politecnico di Torino, 10129 Torino, Italy; edoardo.goti@polito.it
[2] Department of Electrical Engineering and Computer Science, Massachusetts Institute of Technology, Cambridge, MA 02139, USA; wanghz@mit.edu (H.W.); xji08thu@gmail.com (X.J.); jingkong@mit.edu (J.K.)
* Correspondence: andrea.mura@polito.it; Tel.: +39-01-1090-5907

Abstract: Among the amazing properties of graphene, superlubricity is one of the most promising properties. This property can be used in industrial field components to reduce friction without using liquid lubricants, and therefore, improve machines' efficiency and reliability with low environmental impact thanks to the elimination of oil or grease lubricants. In this paper, copper alloy samples for electrical purposes were coated with graphene by four different deposition processes. The investigated synthesis processes are direct grown graphene on bulk Cu, transferred graphene, and self-assembled graphene from graphene flakes. Ball-on-disk tests were performed to evaluate the tribological performance of samples. The aim was to compare the effect on the tribological performance given by different types of coatings, taking also into consideration industrial scalability. Interestingly, not all graphene nano-coatings being compared proved effective in reducing friction and wear in gross sliding conditions. The results show that the cost-effective self-assembled graphene is the longer-lasting nano-coating among those investigated in this work, and can reduce both friction and wear. Tests revealed that graphene coatings can be applied as a solid lubricant, reducing friction up to 78%, and reducing the average wear volume up to 40%.

Keywords: graphene; copper; friction; wear

check for updates

Citation: Goti, E.; Mura, A.; Wang, H.; Ji, X.; Kong, J. Comparison of the Tribological Behaviour of Various Graphene Nano-Coatings as a Solid Lubricant for Copper. *Appl. Sci.* **2023**, *13*, 8540. https://doi.org/10.3390/app13148540

Academic Editor: Aimin Yu

Received: 14 June 2023
Revised: 18 July 2023
Accepted: 21 July 2023
Published: 24 July 2023

Copyright: © 2023 by the authors. Licensee MDPI, Basel, Switzerland. This article is an open access article distributed under the terms and conditions of the Creative Commons Attribution (CC BY) license (https://creativecommons.org/licenses/by/4.0/).

1. Introduction

Friction and wear phenomena are among the primary reasons for the reduced operational efficiency of both mechanical components and electrical components, and may lead to early components replacement.

Lubricants are needed to reduce friction and wear at the interface of sliding parts. As for mechanical components, liquid or semi-solid lubricants (such as oils and grease) have always proved effective. However, traditional lubricants have to meet increasingly stringent performance and environmental compatibility constraints because they are extremely polluting substances when replaced and disposed of. Moreover, lubricants may be incompatible with electrical components due to their insulating properties. For these reasons, there has been a growing interest in solid lubricants and high lubricity coatings, including 2D nanomaterials [1], as an alternative to traditional lubricants. For instance, the papers by Spalvins [2], Zhu et al. [3], Friedrich et al. [4], Vamsi Krisha et al. [5], and Huai et al. [6] provide examples of present and prospective applications of solid lubricants in many fields of industry. In particular, issues related to wear associated to copper electrical contacts is a problem of actual importance that still needs a solution [7–10].

Low friction coatings have many advantages compared to fluid lubricants when applied to reduce friction and wear. No lubrication system is needed in mechanical systems, whose design can be simplified, and no leakages or relubrication issues are present (operation and maintenance are more effortless). On the other hand, troubles may arise when coatings are applied to electrical components like connectors or switches.

Many of them are insulating materials (e.g., ceramics or polymer composites), and their presence would impair the fundamental function of the systems, i.e., to conduct electricity. Efforts are being made to develop conductive low friction coatings and hard coatings to improve tribological properties and reduce wear in electrical devices without impairing their conductive properties. For instance, Schoff et al. [11] provided a broad overview of the electric conductivity properties of many solid coatings, highlighting that the most expedient route to enhance the conductivity of traditional coatings is the inclusion of carbon pigments or other metals pigments while boosting their corrosion resistance too. Islam et al. [12] reported the effect of reinforcement of carbon nanotubes and graphene nanoplatelets on electrical conductivity of plasma-sprayed Al_2O_3 coatings. Among the variety of materials used as friction reduction coatings, graphene layers have been investigated for the past few years by many authors in the scientific literature [13] for both mechanical and electrical applications since it was first isolated in 2004 [14]. Being a carbon compound, graphene is ideal for electrical application, thanks to its extremely high electrical conductivity, while serving as solid lubricant as well. Fascinating lubricant properties are attributed to graphene by Penkov et al. [15], who collected and revised in his paper many results from previous tribological investigations at the nanoscale and macroscale on a number of substrates. Zhang et al. [16] reported that the use of multi-layer graphene coating can effectively reduce the wearing-out of tiny electrical connectors and protect them from tribo-oxidation damage, without affecting the electrical conduction through the pair. Lin et al. [17] explored the synergistic effect of TiN–Ag coating and MLG-rich grease to improve the friction, wear, and conduction of copper connectors. Jabith et al. [18] and Sendhil Kumer et al. [19] studied copper matrix composites and aluminium matrix composites with added graphene, respectively. Their results showed that the presence of graphene enhanced the tribological behaviour while increasing the hybrid composition. The wear performances of other types of composite materials have been investigated in [20,21].

Fewer investigations have addressed graphene as nano-coating for macroscale dry sliding contact conditions on copper alloys. To the best of the authors' knowledge, the essential literature on this topic is represented by the papers referred to below. Yildiz et al. [22] tested graphene transferred to a connecting rod journal bearing and observed that even single-layer graphene could protect the rough substrate surface reducing macroscale wear even under severe conditions despite a relatively high coefficient of friction compared to the bare material. Won et al. [23] investigated the effect of the growth time in CVD graphene on copper. Berman et al. [24,25] tested SLG and MLG graphene coating on steel substrates prepared by CVD and solution-processing in a variety of dry, liquid, and inert gas humid environments. Shi et al. [26] investigated the combined effect of graphene coatings and textured substrates, claiming that the friction-reducing effect of graphene was enhanced by the surface texturing. Bhowmick et al. [27] investigated the role of vacuum and humidity in reducing the sliding friction of a titanium sphere being slid against MLG deposited on Ni and tested in a pin-on-disk setup. Interestingly, the lowest was measured when the tests were conducted in an air atmosphere with 45% RH, and it was argued that in the presence of hydrogen the defects in the carbon network generated during sliding resulted in the sp^2 to sp^3 transformation and amorphization during of the graphene.

The scientific literature also reports several methods to produce graphene sheets for various applications [28], e.g., mechanical delimitation or 'scotch-tape' exfoliation [29], chemical and electrochemical exfoliation of graphite [30,31], unrolling/unzipping of carbon nanotubes (CNTs) [32], arc-discharge in various media [33], inkjet printing [34], solution-processing of graphene flakes with drop-casting of graphene films [24], and others. However, few of them are suitable for the production of continuous graphene sheets large enough to cover wide areas of mechanical or electrical components. Among the others, two methods which promise to meet this requirement were considered for this paper:

- Low-Pressure Chemical Vapor Deposition (LPCVD) on Cu or Ni foils [35,36];
- Self-assembly of graphene nano-platelets (GNPs) via sonication in distilled water [37].

In the previous works of Mura et al. [38–40], these two deposition techniques were compared for the production of graphene layers deposited onto both metallic and polymeric substrates. These results showed that low-quality MLG produced with cost-effective deposition methods usually outperform high-quality and high-purity SLG by CVD in terms of tribological performance.

More recently, Van Sang et al. investigated solid lubricant particles by combining graphene and iron nanoparticles [41] and the lubrication of graphene for the iron contacts [42]. Song et al. [43] and Savjani et al. [44] investigated, respectively, the performance of copper ions in situ incorporated into graphene oxide nanosheet and copper metal matrix composites reinforced with fluorinated graphene oxide nanosheets as coatings as solid lubricant. Buzio et al. [45] analysed wet-transferred solution-processed graphene flakes in solid lubrication. Wang et al. [46] used multi-layer graphene/silicon dioxide coating as solid lubricant, and García-Alonso et al. [47] investigated the tribological behaviour of graphene-based solid lubricants biofunctionalized with hyaluronic acid.

In this paper, copper for electrical purposes is used as a substrate. Four different kinds of coating produced according to the above-mentioned methods were tested. The aim of this work is to investigate how graphene nano-coatings synthesized by different processes can modify the macroscale tribological performance of copper. This would allow identifying the most promising one for those industrial applications where improved friction and wear behaviour are required without impairing the interface conduction, while also considering costs and industrial scalability. Among the others, graphene directly grown on a bulk thick copper substate by CVD is explored, which, to the best of the authors' knowledge, has been investigated only for dielectric substrates [48] and for bulk metals by the authors in a previous paper [49].

This paper is the continuation of a series of comparative investigations by the authors about the macroscale tribological performances of different kinds of graphene nano-coatings deposited on a variety of metallic and polymeric substrates [38–40].

2. Materials and Methods

2.1. Preparation of the Samples and Graphene Nano-Coatings

The material for the tribological samples was a technically pure copper Cu-ETP (EN 13599:2014) widely used for electrical purposes. Table 1 reports the standardized chemical composition of the Cu-ETP copper grade and its mechanical properties. Five rectangular samples of size 12 × 10 mm^2 and about 5 mm thick were cut from a square conductor for electrical cabinets (ItalWeber, Assago, Italy) [50]. The choice of this copper grade is in line with previous experimental investigations [23]. The surface of the samples was prepared by grinding with sandpaper and polishing with diamond slurries to achieve high planarity and a high surface finish. The average roughness was Ra 0.182 µm. After cleaning in an ultrasonic bath with acetone for 10 minutes and drying with a lint-free tissue, samples were coated with graphene. Preparation of samples was performed at the MIT Laboratories (Cambridge, MA, USA).

Table 1. Material properties of the copper substrate.

Chemical Composition					
Cu 99.90%	Bi Max 0.0005%		Pb Max 0.005%	O Max 0.040%	
Mechanical properties					
Tensile strength 220 MPa	Yield strength 160 MPa	Elongation at break 33%	Specific weight 8.89 g/cm^3	Electrical resistivity 0.017 µΩ·m	Hardness HV 100

Four different types of graphene nano-coating were synthesized and deposited on one sample. Five samples were tested overall, including one bare copper sample to identify the reference tribological behaviour of the substrate:

- 1 sample was coated with graphene directly grown onto the bulk copper substrate by APCVD;
- 1 sample was coated with a high-purity graphene sheet synthesized by LPCVD on a Cu foil and then transferred to the end copper sample;
- 1 sample was coated by self-assembled graphene flakes after 3 h of sonication in the DI (see Section 2.1.3), referred to as 3 h-percolative;
- 1 sample was coated by self-assembled graphene flakes after 6 hours of sonication, referred to as 6 h-sonicated;
- 1 bare copper sample.

2.1.1. Transferred CVD Graphene

The thermally activated Chemical Vapor Deposition (CVD) process was performed inside a hot wall fused silica tube reactor (ThermoFisher Scientific Lindberg/Blue M™ Tube Furnace, Waltham, MA, USA) using H_2 as inert gas and methane as the gas-phase precursor of graphene. For the transferred graphene coating, the SLG film was grown on a sacrificial 25 µm thick Cu foil (Alfa Aesar #13382, Shanghai, China), with 99.8% purity, that acted as the metal catalyst body, following a standard low pressure chemical vapor deposition (LPCVD) procedure. After evacuation of air by means of a vacuum pump, the chamber was filled back with hydrogen and heated at 1000 °C keeping pressure to about 120 Pa. Heating was maintained for 30′ for annealing and removing the native oxide on the copper surface as well as to increase the grain size; then a flow of CH_4 (35 sccm) and H_2 (50 sccm) was guaranteed through the chamber for the whole growth time. After cooling to room temperature in pure hydrogen, a layer of ethylene-vinyl-acetate (EVA) was spin-coated on the graphene/copper foil to be used as a transfer supporting layer and baked in the oven at 80 °C. The copper foil was etched away (Copper Etchant TFB, Transense, Oxfordshire, UK) and the resulting EVA/graphene stack was rinsed in DI water. The Eva/graphene stack was subsequently transferred onto the copper sample surface by immersion into the DI water bath, and the sample heated at 80 °C into N_2 environment for one hour so that graphene grabbed onto the metallic surface. Finally, the EVA was removed from the sample using Xylene at 90 °C.

The transferred graphene has a high-quality low-defect structure characterised as about 95% monolayer according to some authors [51,52]. It gives the freedom to cover any kind of substrate, that could be also much rougher [49], but its production in large quantities may be expensive due to the cumbersome transfer process.

2.1.2. Direct Growth Graphene

For the direct growth graphene, Ambient Pressure Chemical Vapor Deposition (APCVD) was performed with slightly different process parameters compared to transferred graphene. The bulk copper sample was loaded into the furnace instead of the cooper foil. The fused silica tube was evacuated and pressurised again to ambient pressure with H2; the temperature was then increased up to 1030 °C in 30′ under 10 sccm flow of hydrogen. The annealing process was also performed by maintaining the bulk copper sample at 1030 °C for 30′. The graphene synthesis started by setting the flow of mixed methane and hydrogen (10 sccm of CH_4 and 100 sccm H_2) through the chamber. After growth, the samples were quickly cooled to room temperature in H_2.

The direct growth process allows synthesizing large-area graphene directly on the sample surface, avoiding the time-consuming transfer process. For this reason, it is of great interest in the perspective of applying high-purity graphene coatings to industrial components directly. To the best of the authors' knowledge, no researcher has ever tried to produce CVD graphene inserting a bulk and thick copper body into the CVD furnace directly. The sole earlier attempt of performing direct growth of graphene on a bulk metallic

body was by Mura et al. [40], who obtained a layer of graphene directly grown on the surface of a bulk steel sample. Direct growth lets one avoid the complicated transfer process, which induces the defects, residues, and tears that degrade the performance of the graphene sheet [48].

2.1.3. Percolative Graphene by Self-Assembly of Graphene Flakes

An Ultrathin Graphene Film (UGF) can be produced by self-assembly of graphene nano-platelets (GNPs). This method is a variant of the solution-processing-based methods of graphene flakes and follows the procedure described by Li et al. [37]. Graphene flakes were prepared in-house by electrochemical exfoliation from a bulk graphite rod (Sigma-Aldrich, Darmstadt, Germany) within an electrolyte solution, applying 10 V bias to a platinum wire as grounded electrode. The flakes were collected by filtration and then dispersed in dimethylformamide. To get high-quality flakes and narrow the flakes thickness distribution, the solution thus obtained was centrifuged to remove side products like thick graphite particles. Centrifuged flakes were re-dispersed in ethanol with a mass concentration of 1 mg/mL and the ethanol solution injected on the surface of the DI water. The graphene flakes spread on the DI water surface due to the Marangoni effect and tied with each other as ethanol evaporated. The shaping of the continuous UGF by the self-assembly process was facilitated by sonicating the DI bath. In this work, two sonication times were tried out: 3 h and 6 h. Previous Raman analysis [38] showed that with increasing the sonication time, the amount of graphene agglomerations increases too. The UGF was transferred onto the sample surface by immersion of the sample into the DI water solution, and the samples were finally dried at 75 °C.

The few-layered graphene structure thus obtained, also called percolative graphene, is said to have high structural uniformity [37], even though it may suffer from clamping-up of flakes due to imperfect binding of flakes. Although relatively cheaper and easier to produce, there are several factors that may potentially play a role in the overall quality of the graphene layer, e.g., size of flakes, quality of flakes, and sonication time.

2.2. Sample Surface Inspection and Tribological Testing

Figure 1a shows the topography of the five samples after preparation and the corresponding value of the 3D areal surface roughness as per ISO 25178. Figure 1b illustrates the appearance of the sample surface under the optical microscope. The significant increment of roughness measured for the sample coated by directly grown graphene is presumably due to the curious globular-like structure observed on the surface of the sample during FESEM analysis (Figure 2). Some details are provided on this aspect in the following sections.

The samples were inspected with FESEM (Zeiss, Jena) with an ultra-high-resolution Inlens EsB detector to image the carbon nano-coatings; images are grouped in Figures 2 and 3. Except for direct growth graphene, a transparent grainy structure was perceived on the surface of the sample through which one can see the roughness pattern of the substrate surface. It corresponds to the ultra-thin layer of sp^2-bonded carbon atoms. The transferred graphene coating appeared as a uniform patchwork with patches of similar colour, and it looked like the bilayer graphene structure reported by Ullah et al. on copper [53]. The patches are single-crystalline graphene islands grown at nucleation sites on the catalyst foil. As for self-assembled graphene coatings, the enlarged images suggested that the recombination of GNPs was effective in covering the surface of the sample, but the pattern of dark and light patches hints that the carbon layer is uneven, as expected, with regions of locally increased thickness due to folds (see also the inset of Figure 3) or superpositions of many flakes. This graphene structure appeared very similar to the eight-layer graphene reported by Ullah et al. [53].

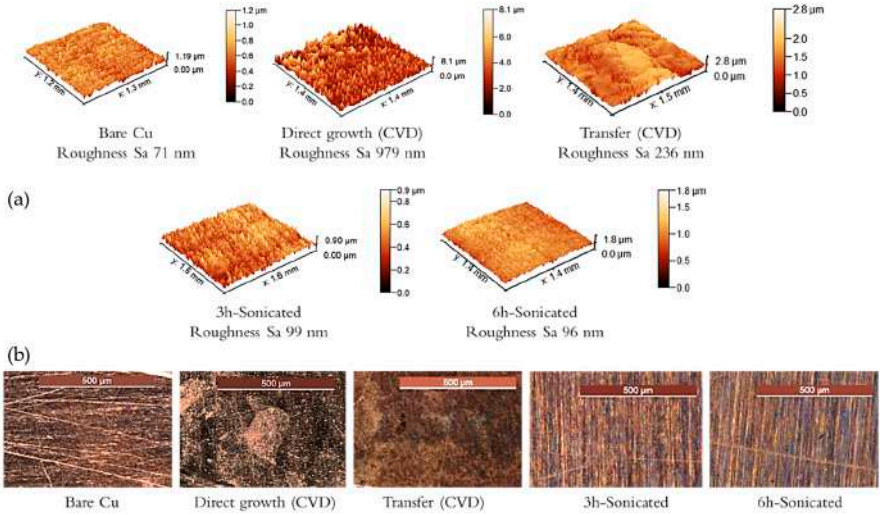


Figure 1. (**a**) Surface morphology of the coated samples before the tribological tests. (**b**) Inspection under the optical microscope of the sample surface before the tribological test. Interestingly, the surface of the samples with direct growth graphene features a pattern of platelets or grains which resembles the morphology of multiplayer CVD graphene on Ni substrate reported by Bhowmick et al. [27]. This led the authors to envisage a growth mode as 'islands' or agglomerations of platelets of different thickness.

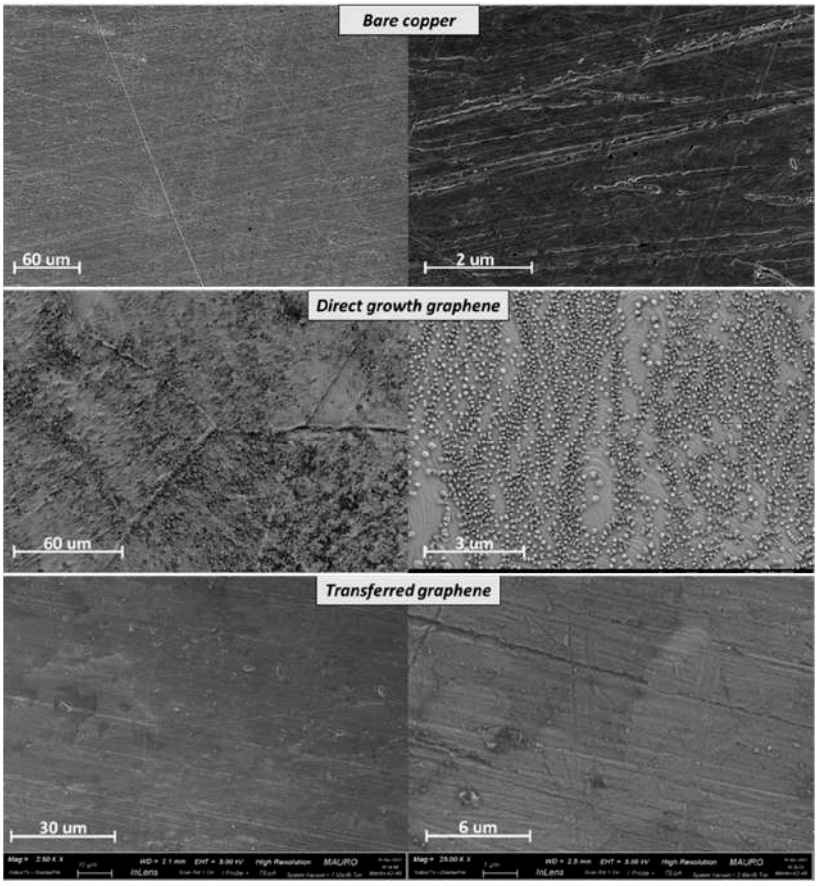


Figure 2. SEM imaging of transferred and directly grown graphene with magnification 500×, 2.5 kX and 25 kX.

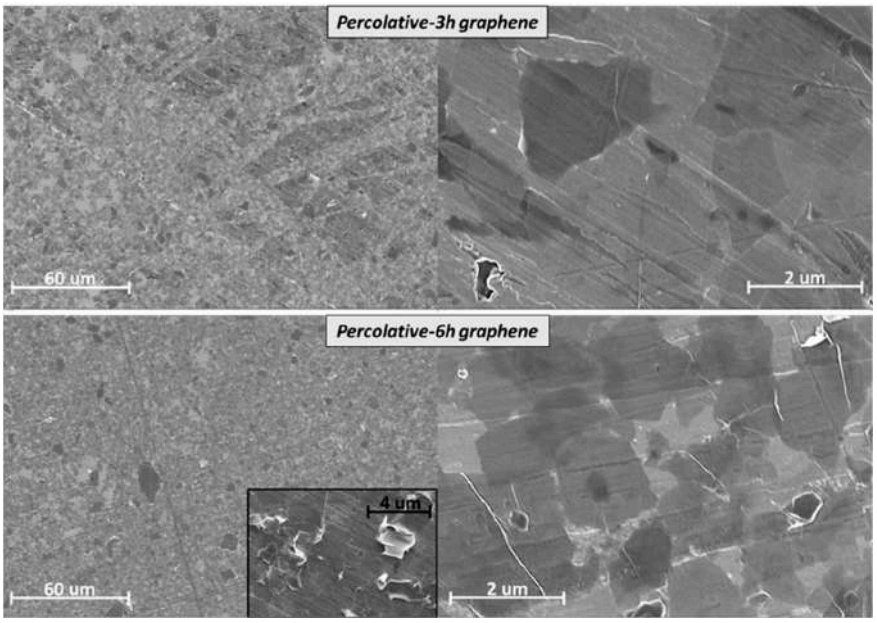


Figure 3. SEM imaging of the percolative graphene nano-coatings with magnification 500× and 15 kX. Inset shows defective recombination of GNPs resulting from the production process of the graphene sheet.

The surface of the direct growth graphene appeared covered by a structure of spherical nodules protruding from the surface. The authors found no other evidence of CVD graphene on copper with a similar surface texture in the scientific literature. A possible explanation of this phenomenon could be that this peculiar globular structure is made of relatively hard amorphous carbon nodules. Hu et al. suggested that amorphous carbon can originate on the surface of copper foils during the CVD process if an insufficient flow of precursor gas is supplied and, thus, an insufficient amount of C solubilizes into the substrate [54]. The concentration of the carbon precursor is an important influencing factor in triggering the graphene nucleation, irrespective of the reactor temperature (800–1000 °C) and the nature of the catalyst metal. This argumentation led the authors to raise the hypothesis that the globular structure visible under FESEM inspection is some form of agglomerated amorphous carbon grown in place of the pristine graphene layer at the nucleation sites. The reasons for this phenomenon are yet unclear. The flow rate or the partial pressure of CH_4 inside the reactor might have been insufficient to promote the supersaturation of C atoms on the surface of a thicker copper substrate compared to the case of deposition on Cu foils. At the same time, the state-of-the-art understanding of the deposition process evidences that carbon solubility decreases with cooling down, and carbon precipitation triggers the surface crystallization of the graphene lattice [55]. Therefore, it might also be that the cooling of the thick copper target inside the reactor after CH_4 inflation was not fast enough to allow for crystallization at the nucleation sites. Deeper investigations are necessary to clarify these aspects in the future.

The higher magnification tilted view FESEM image and the results of the AFM analysis in the centre of the sample supported this hypothesis (Figure 3). The height profile allows quantifying the average size of the nodules equal to about 150 nm high and 300 nm wide.

Therefore, the direct growth CVD process on bulk copper (Figure 4) presented in this research is considered unsuccessful since it did not provide a graphene sheet but a degraded carbonic structure. Nonetheless, the tribological tests performed on the available sample treated by direct growth CVD are presented in Section 3.2. However, the direct growth CVD sample results will not be directly compared to those obtained with actual graphene nano-coatings because it would be meaningless.

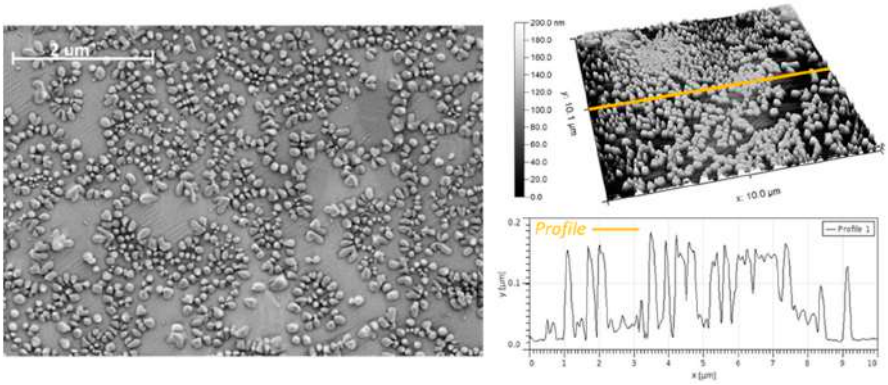


Figure 4. 43 kX FESEM image of the surface of the direct growth sample (on the (**left**)); 10 µm × 10 µm AFM height map in the centre of the sample coated with direct growth graphene (on the (**right**)). The line profile shows the characteristic dimensions of the globular structure.

Optimization of the direct-growth deposition process is needed because little is known in the scientific literature about the optimum deposition parameters for direct growth CVD on bulk metal specimens. No researchers have ever tried to produce CVD graphene by catalysing the reaction with a bulk and thick specimen placed inside the CVD furnace. Unfortunately, there was no time to achieve this optimisation goal within the bounds of this thesis work.

This failure gives the feeling of the challenge related to the scalability of this approach intended to avoid the cumbersome transfer procedure of the graphene sheet. The direct growth process would allow synthesising a graphene layer on the surface of the components directly, avoiding the time-consuming transfer process. For this reason, it is of great interest in the perspective of applying high-purity graphene coatings to industrial components directly.

2.3. Tribological Testing

Tribological testing was performed in air at 27 °C and 33% humidity with a pin-on-disk tribometer (Anton Paar TriTec, Switzerland) against a 6 mm AISI 52100 (100Cr6) steel ball under 2 N load. The tribological characterisation was carried out at Politecnico di Torino and the friction coefficient (CoF) was recorded during the tests. Unidirectional rotating wear tests were run under 2 N load and 15 mm/s speed, and the total sliding distance was 30 m. The selected load and speed conditions aimed to avoid excessive graphene layer damage and wear. Three tribological tests were carried out on each sample with an increasing radius of the wear track, i.e., 2 mm, 3 mm, and 4 mm. The dimension of the specimens prevented running more than three wear tests per sample. Berman et al. [56] argued that graphene protection is more pronounced at lower loads, while under higher loads, the graphene layer is quickly worn out and removed out of the wear track with a reduced beneficial effect for the system. The corresponding average Hertzian contact pressure at the beginning of the test was 336 MPa, calculated via the HertzWin [56] software, considering the effect of roughness on the contact stress state (Ra 0.092 µm for the steel sphere and Ra 0.182 µm for copper). The initial contact pressure was consistent with previous works on the frictional behaviour of graphene coatings [23,24,54].

2.4. Wear Volume Calculation

The surface of the samples was scanned with an InfiniteFocus G5 Focus Variation (FV) 3D digital microscope by Bruker Alicona (Raaba, Austria) with a 20× high-resolution lens to measure the amount of wear. The surface enclosed in the square area around the three concentric wear tracks in Figure 5a was acquired at once to have a single reference plane to estimate the wear volume of the three tracks.

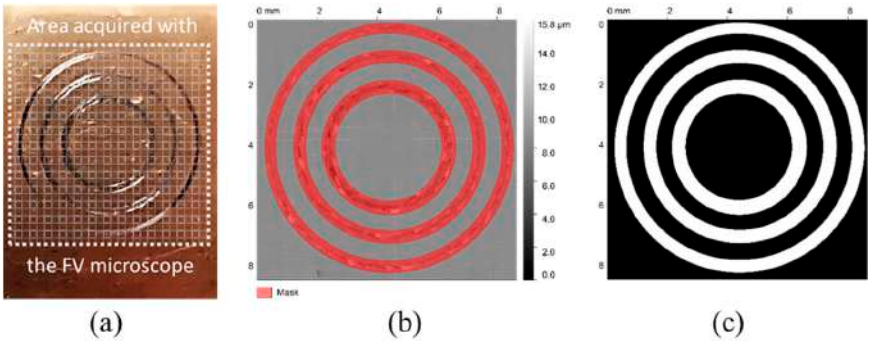


Figure 5. (**a**) Region of the samples scanned with the 3D microscope, (**b**) masks applied to the topographic data, (**c**) binary trace of the masked region.

The volume of removed material and deposited or plastically displaced material were calculated with the Volume Parameters Topographic method based on the Abbott-Firestone curve. The method is schematically represented in Figure 6 and relies on Equations (1)–(3). Further details are reported by Leach [57], Waterworth [58], Genta et al. [59], and Maculotti et al. [60]. This calculation method of the wear volume was proved by Maculotti et al. to be the most robust from a statistical point of view. It has higher accuracy and lower uncertainty than the method suggested by the standard ASTM G99-17 and ISO 18535 based on the profilometry of the wear tracks

$$V_{VP} = V_m(m_r) + V_v(m_r) \tag{1}$$

$$V_m(h_0) = K \int_0^{h_0} S_{mc}(h)dh \tag{2}$$

$$V_v(h_0) = K \int_{h_0}^{1} (1 - S_{mc}(h))dh \tag{3}$$

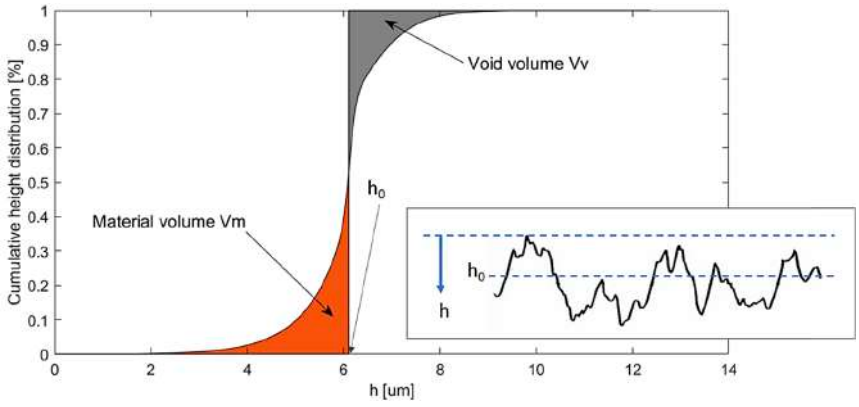


Figure 6. Void and material volume parameters of the Abbott-Firestone curve.

In Equations (1)–(3), V_m and V_v are the material volume and the void volume, respectively, V_{VP} is the total damage volume, h is the surface height, S_{mc} the cumulative probability distribution of the surface heights (i.e., the Abbott-Firestone curve), and K is a conversion factor that represents the area of the projected surface topography on a horizontal plane. Given a specific horizontal section plane representing the average position of the unworn surface whose height is h_0, V_m represents the volume of material enclosed below the measured surface and above this plane, whilst V_v is the volume of missing material above the surface and below this plane.

Volume calculations were performed through the open-source software Gwyddion [61]. Rough topographic datasets were imported into Gwyddion, where three annular masks

identified three regions of interest (ROI), as Figure 5b shows. Setting suitable ROI was necessary to exclude from the volume computations any contributions from roughness and other topographical features of the surrounding surfaces that are not related to the tribological tests. The dataset outside the three annular masks, i.e., the region in black in Figure 5c, was exploited to fit a polynomial function through which the rough topographic acquisition was planarized by shape removal. This practice is imperative to correct the residual error of planarity, and thus, to identify the reference section plane representing the unworn surface accurately. This plane at z = h_0 was identified as the median value of the dataset filled in with black filler in Figure 5c. The Abbott-Firestone curve was computed for each wear track individually by elaborating the data inside each annular region of the mask. The integration of the Abbott-Firestone curve schematically represented in Figure 6 provided the quantification of the material removed and displacement during the sliding interactions.

3. Results and Discussion

3.1. Friction

The effect of graphene on friction is clearly observed in Figure 7. The friction curve related to the bare copper sample (the blue curve) is the reference trend to understand the impact of the carbon coatings. This curve has an initial friction ramp representing the running-in of the sliding contact that brings the CoF to stabilise at about 0.8 after a few metres. Looking at the other curves in the same diagram, it appears evident that the presence of a graphene layer makes the CoF curve deviate from that of the bare copper sample, especially in the first few meters of sliding. All the graphene nano-coatings could reduce the CoF from about 0.7–0.8 to 0.15–0.25. However, this beneficial effect endured relatively shortly. Figure 7b is the zoomed view of the first 7 metres of the tests in Figure 7a, where the difference among the curves is most evident, while Figure 8 displays the whole set of the friction curves for every sample (except those of the direct growth CVD specimen, as anticipated in Section 2.1.2).

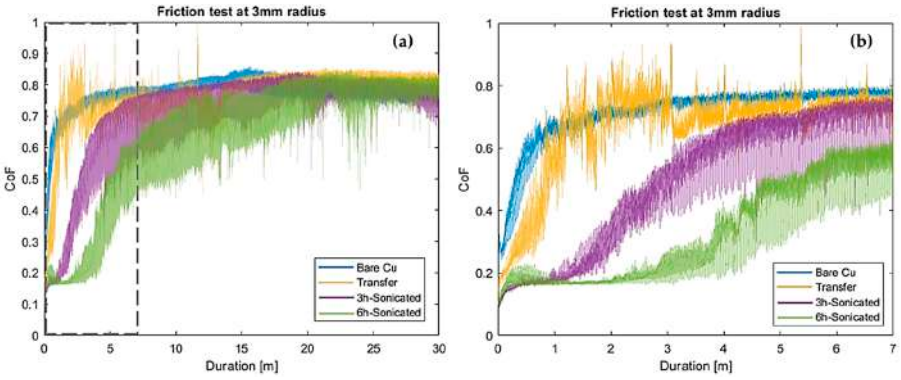


Figure 7. Friction curves measured on the graphene-coated samples at the median radius of 3 mm, (**a**) whole test, (**b**) magnification of forest 7 m.

The friction curves of coated samples can be divided into two parts: Part 1, extending from the beginning of the test to the onset of the friction transition, and Part 2, from transition up to the end of the test.

In Part 1, friction is stable; the friction curves of the graphene-coated samples were flat, featuring a CoF value below 0.2 and low scattering. After this initial phase, a transition occurred that closely resembles the running-in phase observed with bare copper, but delayed by a few metres. The related friction ramp was likely associated with the failure and removal of the graphene coating from the contact region, similar to what was observed in a previous work by the authors [37]. It is accepted among researchers that graphene improves the tribological performance as long as it survives at the interface, because it separates the metal surfaces and reduces the shear stresses at the contact spots of asperities [13,25,53].

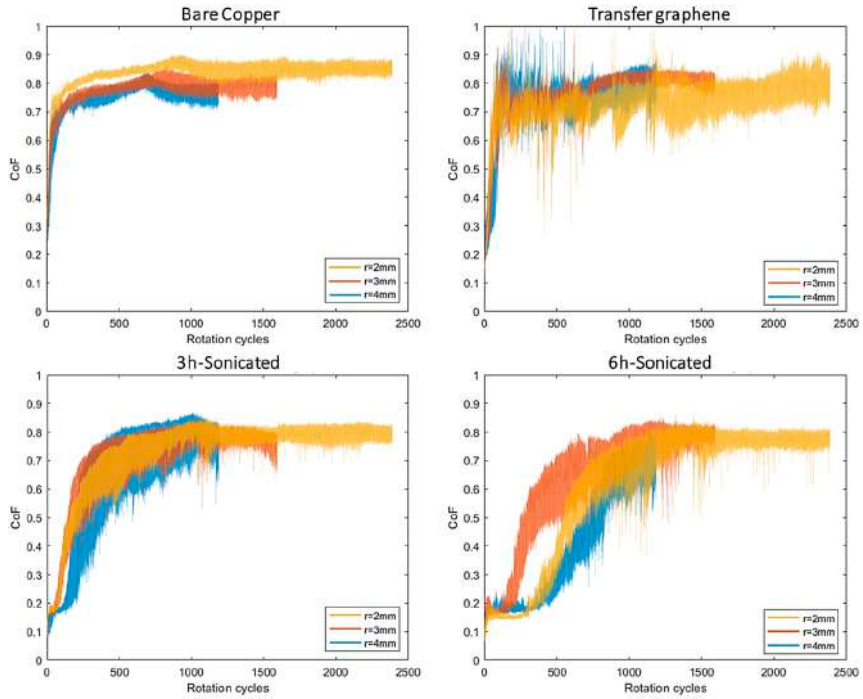


Figure 8. Friction curves from pin-on-disc tests on the graphene-coated samples. Friction curves plotted against the number of rotation cycles allows appreciating the high repeatability of the results despite the different wear track radii.

The duration of Part 1 was strongly correlated to the structure of the coating itself, and, therefore, to shear strength and adhesion. The analysis of the curves in Figure 8 suggests that the transition was completed within just 15 ÷ 20 cycles for transferred graphene. The thickness of the transferred CVD graphene film was so tiny that Part 1 could be hardly distinguished from an ordinary running-in of the steel-copper friction pair. The self-assembled graphene nano-coatings could withstand the tearing-off action of the counter body longer, and the duration was even extended to about 250 cycles on average for the one sonicated 6 h.

Interestingly, irrespective of the initial frictional behaviour, the curves remained always relatively smooth in Part 2 and levelled off in the second half of the test. Both the uncoated and graphene-coated samples had a similar friction value in the last metres of sliding, equal to about 0.8. Only the friction curves of transferred graphene showed some scattering of the friction signal, mainly between 200 and 500 rotating cycles, which may indicate the activation of abrasion and ploughing. Abrasion grooves are evidenced in on this sample, which are indeed not visible inside the wear tracks of the other samples. The other friction curves acquired with bare copper and with the samples coated by self-assembled graphene are much smoother because a transfer layer due to a dominant tribo-oxidative mechanism was established at the interface. Further details are provided in Section 3.2.

The average CoF values measured in Part 1, Part 2, and throughout the whole test are compared in Figure 9. The wearing-out of the self-assembled nano-coatings in Part 1 comes with a stable average friction value equal to 0.17. Interestingly, very similar values were reported in previous research works, as summarized in Table 2. Even with different substrates and environmental conditions, other researchers have recorded friction curves and average friction values with extraordinary similarities to those reported in this research, featuring initial low friction followed by a gradual increase up to the typical CoF of the substrate. Therefore, the value of about 0.17–0.2 should be regarded as the characteristic friction coefficient for the graphene-steel pair regardless of the substrate nature and the characteristic scale of the phenomenon (either microscale or macroscale interaction).

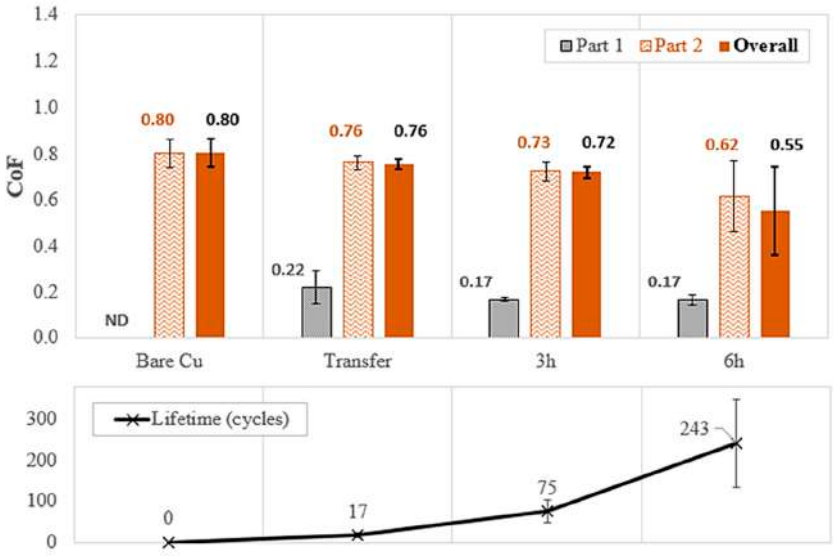


Figure 9. Average CoF values measured in Part 1 and Part 2. The error bars were determined as three times the standard deviation of the average CoF of the three tests carried out with each sample (Lower part). Average lifetime of the coatings determined by the cycles accumulated at the time the transition from Part 1 to Part 2 started.

Table 2. Coefficient of friction of graphene coating reported in previous literature.

Authors	Ref.	CoF	Testing Conditions
Shi et al.	[26]	0.22	Pin-on-disc; graphene-coated and textured M2 steel against stainless steel; 0.5 N load; Testing in ambient air; solution-processed graphene coating;
Berman et al.	[25]	0.19	Pin-on-disc; graphene-coated 440C steel against 440C steel; 2 N load; Testing in ambient air, in ethanol bath and with the addition of droplets of graphene solution; solution-processed graphene coating;
Berman et al.	[24]	0.16–0.23	Pin-on-disc; graphene-coated 440C steel against 440C steel; 1 N load; testing in N_2 and H_2; CVD graphene and solution-processed graphene coating;
Berman et al.	[55]	0.2	Pin-on-disc; graphene-coated steel against steel; 1 N to 5 N load; Testing in dry Nitrogen; solution-processed graphene coating;
Won et al.	[23]	0.2	Pin-on-disc; graphene-coated copper against stainless steel; 20 mN load; Testing in ambient air; CVD graphene;
Yildiz et al.	[22]	0.19–0.4	Flat-on-flat; graphene-coated bronze against AISI52100 steel; 10 N to 30 N load; Testing in ambient air; CVD graphene;
Mura et al.	[38]	0.15–0.25	Pin-on-disc; graphene-coated aluminum against steel; 5 N load; Testing in ambient air; CVD graphene and self-assembled graphene
Mura et al.	[40]	0.15–0.2	Pin-on-disc; graphene-coated steel against steel; 5 N load; Testing in ambient air; CVD graphene

The difference between the average CoF value related to Part 2 and the overall average value of the test is almost null with transfer graphene and 3 h-sonicated self-assembled graphene, because Part 1 lasted very briefly. On the contrary, the 6 h-sonicated self-assembled graphene lasted at the interface long enough to produce a significant 11% reduction of the overall friction coefficient compared to Part 2.

However, when the overall average friction values obtained with the graphene-coated samples are compared to that of bare copper (i.e., comparison of the solid orange columns in Figure 9), some reduction in the CoF was always observed. It was equal to 5% with transferred CVD graphene, and 10% and 31% for 3 h-sonicate dan d 6 h-sonicated self-assembled graphene, respectively. This suggests that graphene was able to provide a beneficial effect to the steel-copper friction pair even after the failure of the nano-coatings.

Interestingly, the SEM analysis (Figure 3) and the results of Raman spectroscopy presented in a previous paper by the authors [38] (it was performed on the same graphene nano-coatings) revealed that the quality of self-assembled UGF was coarse from the point of view of the atomic structure. The coating is a patchwork of several broken atomic layers imperfectly arranged with an uneven thickness distribution. Despite this, the presented results support the evidence that the self-assembled nano-coatings have higher shear strength than high-quality CVD graphene, and are the most promising for tribological applications.

3.2. Wear

The worn surface of the samples after the pin-on-disc tests is shown in Figures 10 and 11, which collect and compare the corresponding topography of the worn-out region acquired with the FV microscope. Samples were blown with air before the topographic analysis, and the wear tracks were gently wiped with a dry lint-free swab to remove any residual wear debris from the surface. The samples were not further cleaned to avoid physical or chemical damage to the carbon layer.

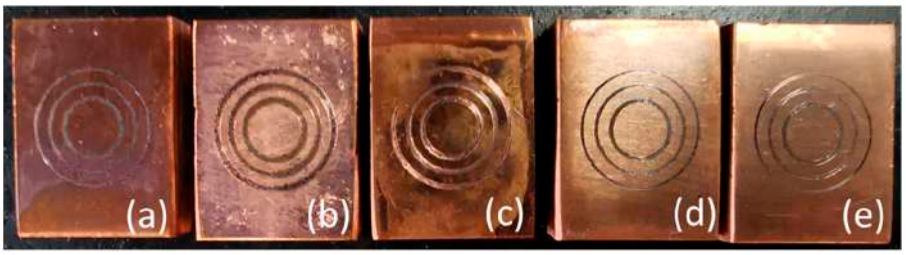


Figure 10. Samples after pin-on-disc tests. (**a**) bare sample, (**b**) directly grown CVD graphene, (**c**) transferred CVD graphene coating, (**d**) 3 h-sonicated graphene, (**e**) 6 h-sonicated graphene. A transparent film adhered to the central part of the metal surface is noticeable on the sample with transferred CVD graphene. The sample with direct growth graphene, whose results will be presented separately in Section 3.2, featured a pattern of bright patches similar to grains visible to the naked eye, probably the contour of the copper grains after annealing.

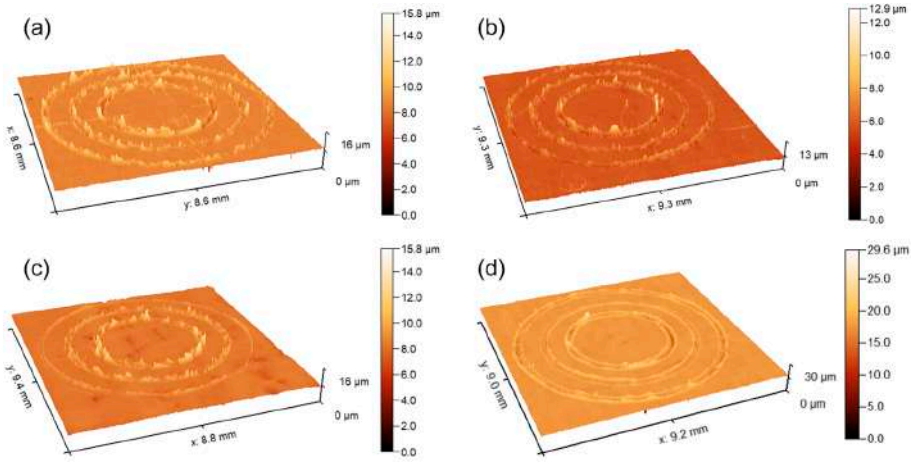


Figure 11. Comparison of the topography acquired with the FV 3D microscope: (**a**) Bare Cu, (**b**) transferred graphene, (**c**) 3 h-sonicated graphene, (**d**) 6 h-sonicated graphene.

As to the counterpart, minor damages appeared on it, and the inspection under the optical microscope provided no evidence of transferred or oxidized matter on the ball. The damage was mostly limited to a local pattern of scratches on the sphere. Therefore, the wearing-out of the sphere was neglected because the related wear volume was not confidently measurable (it was limited to minimal deviations from the initial spherical shape).

The average volume data are presented in detail in Figure 12, and summarized in Table 3. The result of the wear tests revealed different wear behaviours for the various types of graphene coatings.

Table 3. Average value of material loss and deposited/displaced material.

[mm^3]	Bare Cu	Transfer	Percolative-3 h	Percolative-6 h
Average volume of material loss	0.0030	0.0056	0.0019	0.0018
St.Dev. of the volume of material loss	0.0009	0.0022	0.0003	0.0006
Average volume of deposited material	0.0024	0.0045	0.0017	0.0021
St.Dev. of the volume of deposited material	0.0007	0.0014	0.0001	0.0004

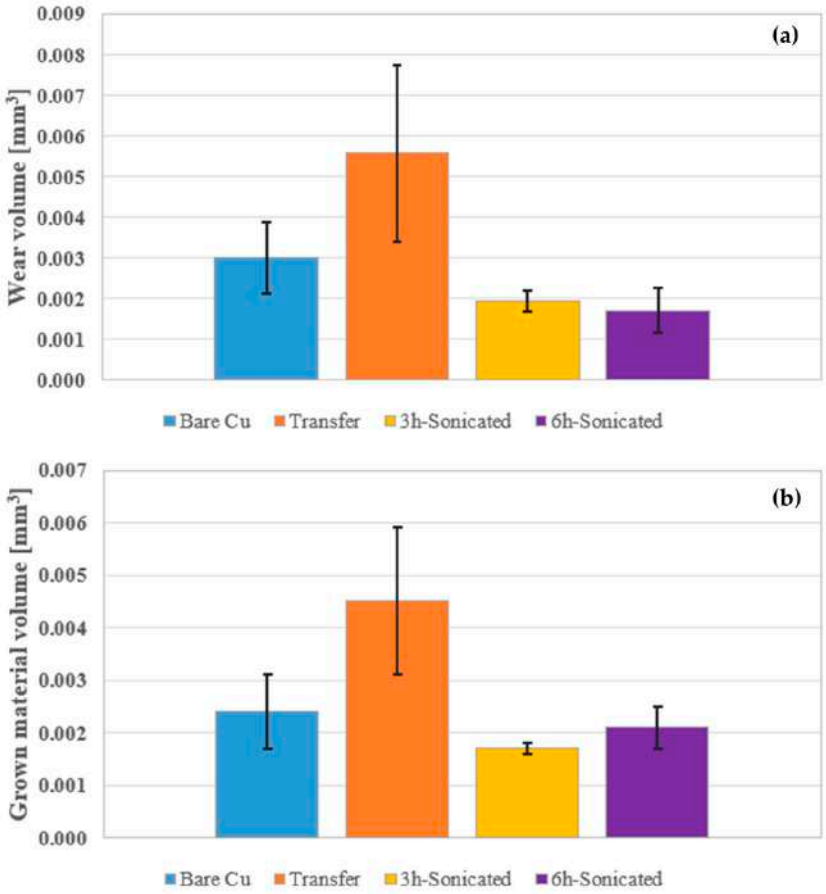


Figure 12. (**a**) Removed material volume and (**b**) deposited or plastically displaced material volume.

The two samples coated by self-assembled graphene performed best, and, in particular, the 6 h-sonicated graphene let the amount of removed material decrease by 36%, taking the bare Cu sample as the reference. The adhered material decreased by 10–15% on average, even though its value was slightly higher for the 2 mm and 3 mm track radii. These results

were remarkably different from those obtained with graphene-coated aluminium samples in a previous work by the authors [37], where no benefits in terms of wear were observed. The relative reduction of wear was substantial, yet the early graphene removal may have hidden the full potential of these coatings if they had endured for a more extended time. The wear volume was measured only at the end of each test, whilst the coating failure happened on average at 1/6th or 1/10th of the total sliding distance. Therefore, the benefits of these high-lubricity graphene nano-coatings might have proven even more significant if the wear volume were inspected repeatedly after shorter sliding distances or at the end of shorter tests.

The performance of transferred graphene was underwhelming. The average amount of lost and transferred material was two times higher than with the bare copper sample. This evidence was surprising because it is not in line with the results of other papers in the scientific literature; for instance, the work by Yildiz et al. [62], who observed a substantial reduction of the wear rate by transferred CVD-graphene.

The morphological analysis in Figure 13 was carried out to investigate the wear mechanisms acting at the tribological interface. The dominant wear mechanisms appeared to change from sample to sample, and were influenced by the production method of the graphene nano-coatings. The wear tracks on bare copper and the percolative-graphene-coated samples have a rather uneven width in the circumferential direction, and feature isolated deeps and hills, suggesting the detachment of chunks of material due to local adhesion and subsequent deposition of oxidized matter inside the sliding path. This is also clearly visible in Figure 14, which shows that a dark grey third layer made of oxidized matter covered the wear tracks, and was responsible for the peculiar morphology visible in Figure 13. Therefore, tribo-oxidation activated by initial adhesion was probably the primary wear mechanism here. In the presence of graphene, this layer may have encapsulated lubricious carbon matter and protected the substrate from wear.

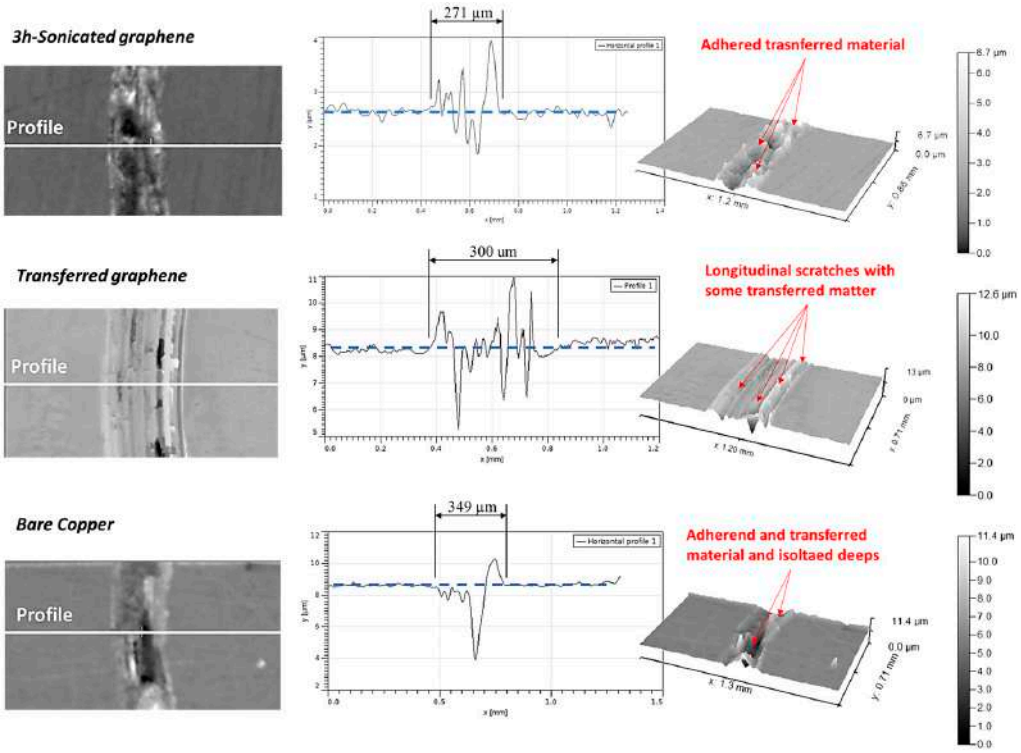


Figure 13. Analysis of the wear tracks morphology. The wear tracks of the tests performed at 3 mm radius were considered for this comparative analysis.

This was not the case for the transferred CVD graphene. The wear track featured a uniform width in the circumferential direction and the presence of longitudinal grooves

and ridges suggested that an abrasion wear mechanism has a role here. Few traces of grey adhered matter were visible inside the wear track, and shining areas of copper were still visible by the end of the test in Figure 14f. Therefore, no transfer layer stabilised at the contact interface, and tribo-oxidation had a limited effect. Abrasion was well correlated with the friction curve recorded during the tests, which were more erratic than the others and characterised by higher scattering of the CoF. Moreover, the contribution of abrasion to wear may also justify the higher wear volume measured with this sample. Abrasion might be activated by the presence of wrinkles and ripples in the transferred graphene layer. According to Long et al., wrinkles and ripples are relatively common in graphene produced by CVD due to the negative thermal expansion coefficient of graphene. Wrinkles appear during the cooling process as the substrate shrinks while the coating dilates [63]. Paronyan et al. [64] also pointed out that the critical phase of the CVD method is the cooling-down of the Cu-C system, since at about 1000 °C, a thin melted layer is likely to appear on top of the catalyst body and it may run into quenching. Such undercooling is responsible for forming a surface Cu lattice favourable to many graphene ripples, e.g., ripples formed due to cellular and dendritic solidification patterns. Comanescu [65] proved that transfer from the copper foil to a super smooth surface (like SiO_2) might make the graphene sheets flatter and less defective. However, if some ripples formed during the CVD process, they could be easily transferred to the end copper sample because the surface finish of these samples was much higher than those employed by Comanescu. The high shear stress experienced by the wrinkles and ripples under sliding contact interactions may lead to structural changes from sp^2 to amorphous carbon, according to Huang et al. [66], leading to harsher tribological conditions.

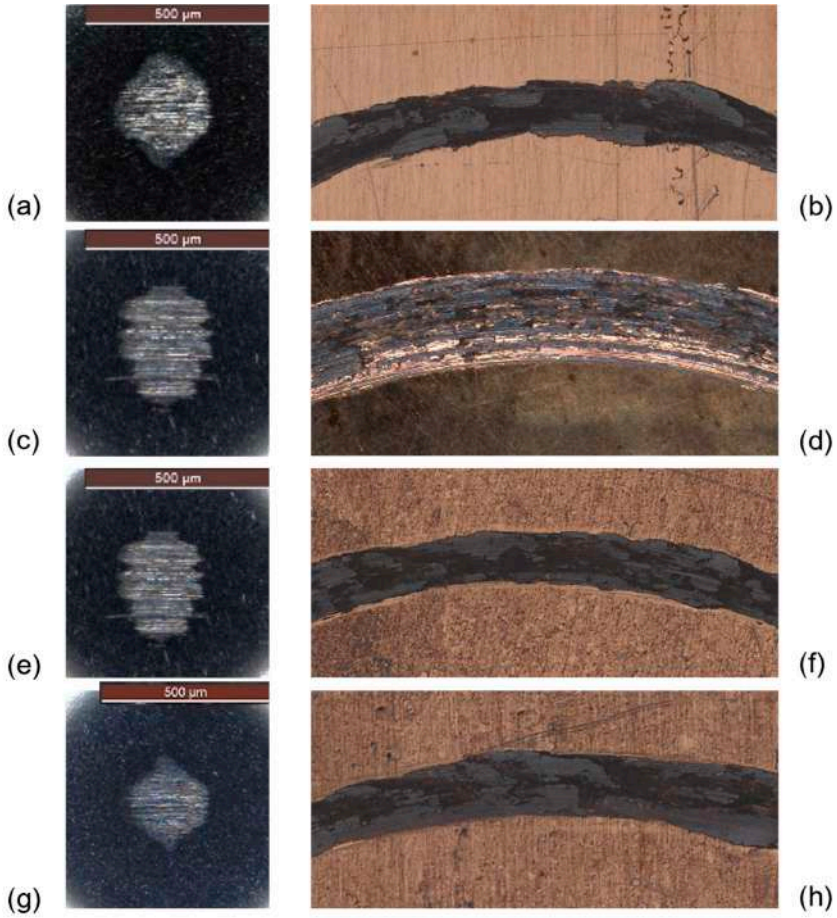


Figure 14. (**a**) Wear scars on the steel balls (**left**) and wear tracks on the copper samples (**right**). (**a**,**b**) Bare Cu, (**c**,**d**) transferred graphene, (**e**,**f**) 3 h-sonicated graphene, (**g**,**h**) 6 h-sonicated graphene.

The analysis of the roughness values measured inside the wear tracks after the tests are presented in Table 4. Interestingly, the roughness values were higher than the initial ones and correlated with the inherent wear results. Lower *Sa* values than bare Cu were measured for the two samples with the best tribological performance, and higher *Sa* for the other two, which supports the evidence that graphene had a beneficial lubricious effect only in the form of percolative graphene, at least in the sliding contact conditions explored in this research. The *Sa* and *Sq* surface roughness parameters were calculated after extracting a random region inside the wear track and removing the waviness shape through a polynomial function. This evidence agrees with the results by Won et al. [23], who claimed a reduction in the average roughness and width of the wear tracks when the tribological performance was enhanced by graphene.

Table 4. Average roughness value inside wear tracks and track width.

		Bare Cu	Transfer	Percolative-3 h	Percolative-6 h
Initial roughness value	*Sa* [μm]	0.071	0.236	0.098	0.096
Roughness inside wear tracks	*Sa* [μm]	0.671	0.957	0.508	0.525
	Sq [μm]	0.897	1.514	0.641	0.701
Wear track width	[μm]	349	300	271	231

3.3. Direct Growth CVD

As to direct growth CVD, the specimen disclosed different tribological behaviour against the steel sphere. Figure 15a compares the friction curve of the direct growth sample with the other friction curves of bare copper and graphene-coated copper samples. High friction was measured at the beginning of the test, with a peak of 1.4 at the onset of sliding. A gradual decrease of the CoF followed, and stabilisation at a value slightly lower than the other curves of the diagram. The friction curves in Figure 15b suggest that an additional abrasive effect worked at the interface at the beginning of the test, which was detrimental to the tribological system. The amount of material removed and displaced was also distinctly and dramatically higher than the uncoated sample. The wear volume calculations are presented in Figure 16 and Table 5. No previous investigation about samples prepared by direct growth CVD reported a similar result.

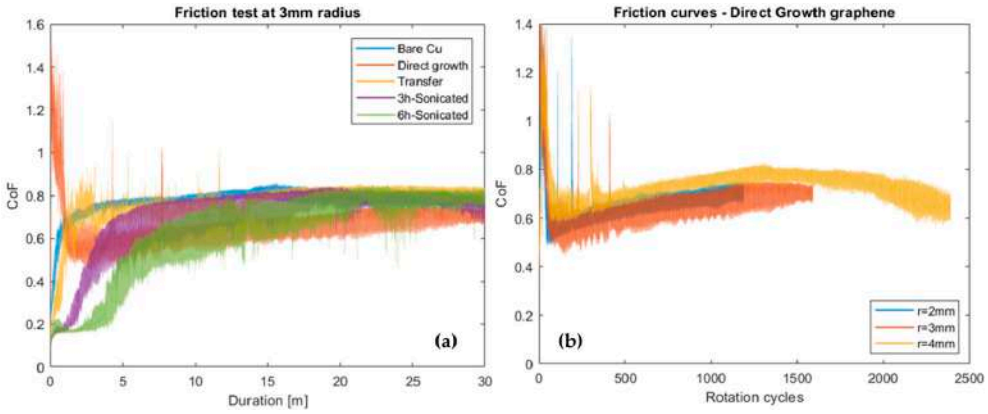


Figure 15. (**a**) Friction curves were measured with the sample treated by direct growth CVD and compared to the other samples at the median radius of 3 mm. (**b**) Set of friction curves measured with the direct growth sample.

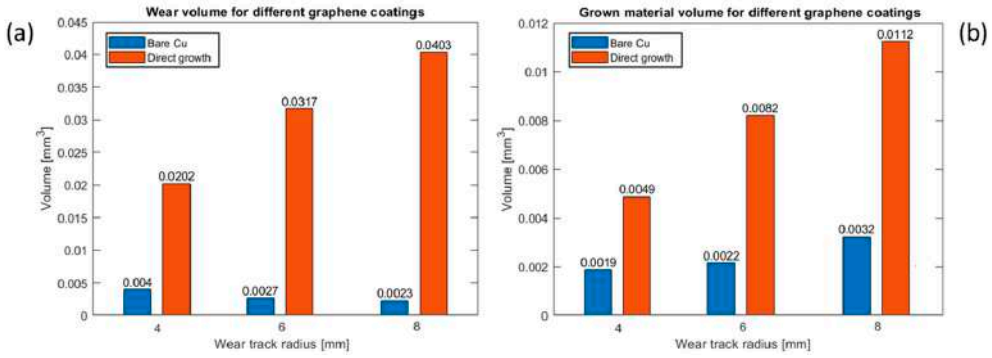


Figure 16. (**a**) Removed material volume and (**b**) deposited or plastically displaced material volume for the direct growth sample.

Table 5. Average value of material loss and deposited/displaced material for the direct growth sample. Comparison of the roughness value before and after the tribological test.

Direct Growth				
	[mm³]			**[µm]**
Average volume of material loss	0.0307	Initial roughness value	*Sa*	0.979
St.Dev. of the volume of material loss	0.0101	Roughness inside wear tracks	*Sa*	1.176
Average volume of deposited material	0.0082		*Sq*	1.636
St.Dev. of the volume of deposited material	0.0032	Wear track width		578

If hard amorphous carbon formed due to anomalous activation of the carbon nucleation sites, as hypothesised, it is likely that a two-body abrasive effect played a role. Abrasion would justify the peak of the CoF in the very first cycles of the test. During the subsequent downfall of the CoF, the globular structure may have detached and turned into hard debris rolling at the interface. Hard globules may have mixed with copper oxides and strengthened the third layer covering part of the wear track. Some oxidized matter is visible in the middle of the wear in Figure 17b. This scenario would explain, on the one hand, why significant material loss continued up to the end of the test, and, on the other hand, would justify the slightly lower friction coefficient observed in the steady-state part of the tests compared to the other samples.

Figure 17 shows that the wear track was large and deep with no longitudinal scratches. Many recesses distributed along the track are shown in Figure 17c, together with chunks of material ripped off the samples (Figure 17a). These pieces of evidence suggest that after the transition of the CoF, the dominant wear mechanism evolved from dominant abrasion to a mix of adhesion, abrasion, and tribo-oxidation. The wear tracks of the direct growth sample also feature the largest amount of plastically displaced material forming hills at the borders of the tracks, which explains why the wear scar on the ball has high ellipticity in Figure 17a. This effect might be related to the substrate softening due to annealing at high temperatures (1000 °C) during the CVD treatment.

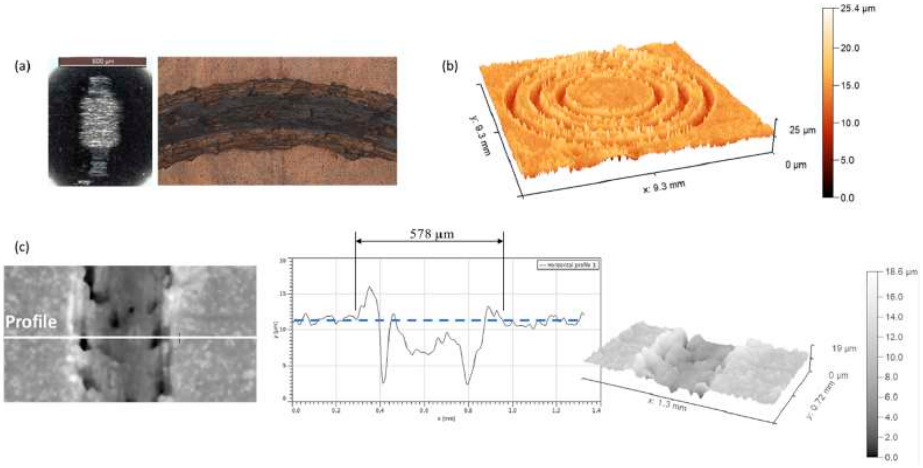


Figure 17. Morphological analysis of the wear track after the tribological test with the sample treated by direct growth CVD. (**a**) chunks of material ripped off the samples, (**b**) 3D measurement, (**c**) wear track measurement.

4. Conclusions

In this work, the tribological performance of graphene-coated copper was investigated. Four methods to synthesize 2D carbon coatings by either transfer or self-assembly of flakes were compared. The nature and quality of the graphene structures thus obtained were investigated through FESEM analysis and compared to Raman spectra to confirm the defectiveness of the layer, and the uniformity of substrate coverage.

The results of the macroscale tribological tests against a steel sphere under low load and low sliding speed revealed that graphene coatings could serve as a solid lubricant while reducing friction and wear of copper. However, the duration of the graphene coatings at the sliding interface was limited because of the limited adhesion to the substrate.

- Self-assembled graphene nano-coatings lasted longer with duration up to 1/6th of the total sliding distance of the test in the case of 6 h-sonicated graphene;
- The CoF dropped from 0.6–0.7 to 0.15–0.25 in the presence of graphene, with a maximum reduction by 78% in the case of 6 h-sonicated graphene. However, this beneficial effect endured as long as the carbon nano-sheet withstood the tearing-off effect of the counter body sliding against it;
- 6 h-sonicated graphene also produced a beneficial 31% reduction of the overall average friction value of the test, despite the short lifetime of the nano-coating;
- The reduction in the average wear volume of copper was remarkable in the case of self-assembled graphene coatings (UGFs). The reduction was about 36% and 40% for the 3 h-sonicated and 6 h-sonicated coatings compared to the bare copper, respectively;
- Transferred CVD graphene showed no benefits on friction and produced a detrimental increase of wear volume, which was never reported in the previous literature.
- The morphological analysis of wear tracks suggested that abrasion had a role in the presence of the transferred graphene layer, while tribo-oxidation dominated in the presence of self-assembled graphene;
- The deposition of direct growth graphene on copper samples failed due to issues likely related to the use of a bulk catalytic body rather than a thin copper foil. Direct growth of CVD graphene on copper samples could not be compared to transferred CVD graphene.

In the end, the results of this research suggested that:

(1) Graphene synthesised through different production methods may contribute to activate different wear mechanisms at the sliding interface;

(2) Graphene obtained from the self-assembly of GNPs is the most promising graphene production method for tribological applications in industry, despite its defective and uneven carbon structure;
(3) Ultra-thin, high-purity, and low-defect structures like transferred CVD graphene are of little interest for macroscale friction and wear applications where gross sliding dominates. It turned out to be overly thin and weak;
(4) The main benefits of self-assembled graphene are its increased thickness and the ability to promote a lubricious third layer at the steel-copper interface;
(5) The synthesis of the direct growth of CVD graphene on bulk metal substrates, which is a promising way to reduce the cost of CVD graphene, needs further investigation to optimize the deposition process route.

Self-assembled graphene coatings are easy to apply, and cost-effective compared to CVD graphene. Nevertheless, the critical aspect for their extensive use in tribological applications is poor adhesion, which limits their endurance against a sliding counter body. Previous research on graphene at the nanoscale [67] has proved that the weak bonding to the substrate cannot prevent ripples and puckers in the out-of-plane direction from arising in front of the contact. The functionalization of the substrate surface, e.g., by plasma etching, to enhance adhesive attraction can be a promising way to strengthen graphene nano-coatings [68] and to extend its duration in contacts subjected to gross sliding.

Moreover, graphene coatings may have higher performance in contact conditions involving limited rubbing motion (either in time or amplitude), e.g., where fretting dominates, or in cold metal-forming processes. Based on these results, comparative fretting tests with the same kind of graphene-coated samples will be performed in the future.

Author Contributions: Conceptualization, J.K. and A.M.; methodology, A.M. and E.G.; validation, A.M. and E.G.; formal analysis, E.G.; investigation, H.W., X.J. and E.G.; resources, J.K. and A.M; data curation, E.G.; writing—original draft preparation, E.G. and A.M; writing—review and editing, E.G. A.M, H.W., H.W. and J.K.; visualization, E.G.; supervision, A.M. and J.K.; project administration, A.M. and J.K. All authors have read and agreed to the published version of the manuscript.

Funding: This research received no external funding.

Institutional Review Board Statement: Not applicable.

Informed Consent Statement: Not applicable.

Data Availability Statement: Not applicable.

Acknowledgments: The authors acknowledge MITOR-MISTI Project 2016 for supporting the collaboration between the MIT and PoliTo research groups. The authors would like to thank Bruker Alicona Italia for performing the 3D microscopic acquisition. The authors appreciated their invaluable help in providing the 3D surface topography of the worn-out samples.

Conflicts of Interest: The authors declare no conflict of interest.

References

1. Uzoma, P.C.; Hu, H.; Khadem, M.; Penkov, O.V. Tribology of 2D Nanomaterials: A Review. *Coatings* **2020**, *10*, 897. [CrossRef]
2. Spalvins, T. Coatings for wear and lubrication. *Thin Solid Film.* **1978**, *53*, 285–300. [CrossRef]
3. Zhu, M.; Zhou, Z. An investigation of molybdenum disulfide bonded solid lubricant coatings in fretting conditions. *Surf. Coat. Technol.* **2001**, *141*, 240–245. [CrossRef]
4. Friedrich, K.; Schlarb, A. *Tribology of Polymeric Nanocomposites: Friction and Wear of Bulk Materials and Coatings*; Elsevier: Amsterdam, The Netherlands, 2011.
5. Krishna, P.V.; Srikant, R.; Rao, D.N. Solid lubricants in machining. *Proc. Inst. Mech. Eng. Part J* **2011**, *225*, 213–227. [CrossRef]
6. Huai, W.; Zhang, C.; Wen, S. Graphite-based solid lubricant for high-temperature lubrication. *Friction* **2021**, *9*, 1660–1672. [CrossRef]
7. Liu, X.-L.; Cai, Z.-B.; Xiao, Q.; Shen, M.-X.; Yang, W.-B.; Chen, D.-Y. Fretting wear behavior of brass/copper-graphite composites as a contactor material under electrical contact. *Int. J. Mech. Sci.* **2020**, *184*, 105703. [CrossRef]
8. Liu, X.; Cai, Z.; Liu, S.; Wu, S.; Zhu, M. Influence of Wear Test Parameters on the ElectricalContact Performance of Brass Alloy/Copper Contactors under Fretting Wear. *JMEPEG* **2019**, *28*, 817–827. [CrossRef]

9. Parka, C.; Jungb, D.; Chunc, E.-J.; Ahna, S.; Jangd, H.; Kimb, Y.-J. Effect of laser shock peening without coating on fretting corrosion of copper contacts. *Appl. Surf. Sci.* **2020**, *514*, 145917. [CrossRef]
10. Siddaiah, A.; Kasar, A.K.; Khosla, V.; Pradeep, L. Menezes, In-Situ Fretting Wear Analysis of Electrical Connectors for Real System Applications. *J. Manuf. Mater. Process.* **2019**, *3*, 47. [CrossRef]
11. Schoff, C. Coatings clinic: Electrical properties II—Conductivity of solid coatings. *CoatingsTech* **2007**, *4*, 80.
12. Islam, A.; Mukherjee, B.; Sribalaji, M.; Rahman, O.A.; Arunkumar, P.; Babu, K.S.; Keshri, A.K. Role of hybrid reinforcement of carbon nanotubes and graphene nanoplatelets on the electrical conductivity of plasma sprayed alumina coating. *Ceram. Int.* **2018**, *44*, 4508–4511. [CrossRef]
13. Berman, D.; Erdemir, A.; Sumant, A. Graphene: A new emerging lubricant. *Mater. Today* **2014**, *17*, 31–42. [CrossRef]
14. Novoselov, S. Graphene: Materials in the flatland (Nobel Lecture). *Angew. Chem. Int. Ed. Engl.* **2011**, *50*, 6986–7002. [CrossRef]
15. Penkov, O.; Kim, H.-J.; Kim, D.-E. Tribology of graphene: A review. *Int. J. Precis. Eng. Manuf.* **2014**, *15*, 577–585. [CrossRef]
16. Zhang, S.; Arfaei, B.; Chen, Z. Friction force reduction for electrical terminals using graphene coating. *Nanotechnology* **2021**, *32*, 035704. [CrossRef]
17. Lin, F.; Xia, Y.; Feng, X. Conductive and tribological properties of TiN-Ag composite coatings under grease lubrication. *Friction* **2021**, *9*, 774–788. [CrossRef]
18. Jabinth, J.; Selvakumar, N. Enhancing the mechanical, wear behaviour of copper matrix composite with 2V-Gr as reinforcement. *Proc. Inst. Mech. Eng. Part J* **2021**, *235*, 1405–1419. [CrossRef]
19. SKumar, S.; Kumar, S.D.; Magarajan, U. Investigation of mechanical and wear behaviour of graphene reinforced aluminium alloy 6061 metal matrix composite. *Kov. Mater.* **2020**, *58*, 341–349.
20. Zaghloul, M.M.Y.; Veidt, M.; Heitzmann, M.T. Mechanical and Tribological Performances of Thermoplastic Polymers Reinforced with Glass Fibres at Variable Fibre Volume Fractions. *Polymers* **2023**, *15*, 694. [CrossRef]
21. Zaghloul, M.M.Y.; Steel, K.; Veidt, M.; Heitzmann, M.T. Wear behaviour of polymeric materials reinforced with man-made fibres: A comprehensive review about fibre volume fraction influence on wear performance. *J. Reinf. Plast. Compos.* **2022**, *41*, 215–241. [CrossRef]
22. Yildiz, B.; Balkanci, A.; Ovali, I.; Ünlü, C.G. Investigation of tribological behaviours of graphene-coated journal bearing. *Tribol. Mater. Surf. Interfaces* **2018**, *12*, 177–185. [CrossRef]
23. Won, M.-S.; Penkov, O.; Kim, D.-E. Durability and degradation mechanism of graphene coatings deposited on Cu substrates under dry contact sliding. *Carbon* **2013**, *54*, 472–481. [CrossRef]
24. Berman, D.; Deshmukh, S.; Sankaranarayanan, S. Extraordinary Macroscale Wear Resistance of One Atom Thick Graphene Layer. *Adv. Funct. Mater.* **2014**, *24*, 6640–6646. [CrossRef]
25. Berman, D.; Erdemir, A.; Sumant, A. Few layer graphene to reduce wear and friction on sliding steel surfaces. *Carbon* **2013**, *54*, 454–459. [CrossRef]
26. Shi, Z.; Shum, P.; Wasy, A.; Zhou, Z.; Li, L.K.-Y. Tribological performance of few layer graphene on textured M2 steel surfaces. *Surf. Coat. Tech.* **2016**, *296*, 164–170. [CrossRef]
27. Bhowmick, S.; Banerji, A.; Alpas, A. Role of humidity in reducing sliding friction of multilayered graphene. *Carbon* **2015**, *87*, 374–384. [CrossRef]
28. Alami, A.H.; Aokal, K.; Olabi, A.G.; Alasad, S.; Aljaghoub, H. Applications of graphene for energy harvesting applic ations: Focus on mechanical synthesis routes for graphene production. *Energy Sources Part A Recovery Util. Environ. Eff.* **2021**. [CrossRef]
29. Knieke, C.; Berger, A.; Voigt, M. Scalable production of graphene sheets by mechanical delamination. *Carbon* **2010**, *48*, 3196–3204. [CrossRef]
30. Stafford, J.; Patapas, A.; Uzo, N. Towards scale-up of graphene production via nonoxidizing liquid exfoliation methods. *AIChE J.* **2018**, *64*, 3246–3276. [CrossRef]
31. Shi, P.; Guo, J.; Liang, X.; Cheng, S.; Zheng, H.; Wang, Y.; Chen, C.; Xiang, H. Large-scale production of high-quality graphene sheets by a non-electrified electrochemical exfoliation method. *Carbon* **2018**, *126*, 507–513. [CrossRef]
32. Mohammadi, S.; Kolahdouz, Z.; Darbari, S.; Mohajerzadeh, S.; Masoumi, N. Graphene formation by unzipping carbon nanotubes using a sequential plasma assisted processing. *Carbon* **2013**, *52*, 451–463. [CrossRef]
33. Chen, Y.; Zhao, H.; Sheng, L. Mass-production of highly-crystalline few-layer graphene sheets by arc discharge in various H 2-inert gas mixtures. *Chem. Phys. Lett.* **2012**, *538*, 72–76. [CrossRef]
34. Shin, K.-Y.; Hong, J.-Y.; Jang, J. Micropatterning of graphene sheets by inkjet printing and its wideband dipole-antenna application. *Adv. Mater.* **2011**, *23*, 2113–2118. [CrossRef]
35. Li, X.; Cai, W.; Colombo, L.; Ruoff, R.S. Evolution of Graphene Growth on Ni and Cu by Carbon Isotope Labeling. *Nano Lett.* **2009**, *9*, 4268–4272. [CrossRef]
36. Kim, K.S.; Zhao, Y.; Jang, H.; Lee, S.Y.; Kim, J.M.; Kim, K.S.; Ahn, J.H.; Kim, P.; Choi, J.Y.; Hong, B.H. Large-scale pattern growth of graphene films for stretchable transparent electrodes. *Nature* **2009**, *457*, 706–710. [CrossRef]
37. Li, X.; Yang, T.; Yang, Y.; Zhu, J.; Li, L.; Alam, F.E.; Li, X.; Wang, K.; Cheng, H.; Lin, C.-T.; et al. Large-Area Ultrathin Graphene Films by SingleStep Marangoni Self-Assembly for Highly Sensitive Strain Sensing Application. *Adv. Funct. Mater.* **2016**, *26*, 1322–1329. [CrossRef]
38. Mura, A.; Canavese, G.; Goti, E.; Rivolo, P.; Wang, H.; Ji, X.; Kong, J. Effect of different types of graphene coatings on friction and wear performance of aluminum alloy. *Mech. Adv. Mater. Struct.* **2020**, *29*, 539–547. [CrossRef]

39. Mura, A.; Adamo, F.; Wang, H.; Leong, W.S.; Ji, X.; Kong, J. Investigation about tribological behavior of ABS and PC-ABS polymers coated with graphene. *Tribol. Int.* **2019**, *134*, 335–340. [CrossRef]
40. Mura, A.; Wang, H.; Adamo, F.; Kong, J. Graphene coatings to enhance the tribological performance of steel. *Mech. Adv. Mater. Struct.* **2019**, *28*, 657–664. [CrossRef]
41. Van Sang, L.; Sugimura, N.; Khajeh, K.; Washizu, H. Solid Lubricants of Combined Graphene and Iron Nanoparticles for Study of Friction and Stability. *Langmuir* **2022**, *38*, 1860–1868. [CrossRef]
42. Van Sang, L.; Sugimura, N.; Washizu, H. Graphene as solid lubricant vertically buried into iron contact surface by annealing for superlubricity. *Tribol. Int.* **2022**, *165*, 107288. [CrossRef]
43. Song, H.; Zhao, S.; Chen, P.; Mai, Y. Copper ions cross-linking graphene oxide nanosheet coatings towards robust solid lubricants. *Diam. Relat. Mater.* **2022**, *130*, 109453. [CrossRef]
44. Savjani, N.; Mercadillo, V.O.; Hodgeman, D.; Paterakis, G.; Deng, Y.; Vallés, C.; Anagnostopoulos, G.; Galiotis, C.; Bissett, M.A.; Kinloch, I.A. Tribology of Copper Metal Matrix Composites Reinforced with Fluorinated Graphene Oxide Nanosheets: Implications for Solid Lubricants in Mechanical Switches. *ACS Appl. Nano Mater.* **2023**, *6*, 8202–8213. [CrossRef] [PubMed]
45. Buzio, R.; Gerbi, A.; Bernini, C.; Repetto, L.; Silva, A.; Vanossi, A. Dissipation Mechanisms and Superlubricity in Solid Lubrication by Wet-Transferred Solution-Processed Graphene Flakes: Implications for Micro Electromechanical Devices. *ACS Appl. Nano Mater. Artic. ASAP* **2023**, *6*, 11443–11454. [CrossRef] [PubMed]
46. Wang, W.; Chang, W.; Ding, S.; Qu, Y.; Gao, Y.; Wang, K. Preparation and tribological properties of multi-layer graphene/silicon dioxide composites-based solid lubricant coatings at elevated temperatures. *R. Soc. Open Sci.* **2023**, *10*, 220740. [CrossRef]
47. García-Alonso, M.C.; Chico, B.; Lozano, R.M.; Escudero, M.L. Tribocorrosion behavior of graphene-based solid lubricants biofunctionalized with hyaluronic acid on CoCr surfaces. *Tribol. Int.* **2023**, *183*, 108420. [CrossRef]
48. Pham, V. Direct Growth of Graphene on Flexible Substrates toward Flexible Electronics: A Promising Perspective. *arXiv* **2018**, arXiv:1712.09714.
49. Hong, J.; Shin, Y.C.; Zubair, A.; Mao, Y.; Palacios, T.; Dresselhaus, M.S.; Kim, S.H.; Kong, J. A rational strategy for graphene transfer on substrates with rough features. *Adv. Mater. Weinh.* **2016**, *28*, 2382–2392. [CrossRef]
50. Copper Bars and Accessories. Available online: https://www.italweber.it/files/catalogue/pdf/14_Isoflex.pdf (accessed on 28 February 2023).
51. Guermoune, A.; Chari, T.; Popescu, F.; Sabri, S.S.; Guillemette, J.; Skulason, H.S.; Szkopek, T.; Siaj, M. Chemical vapor deposition synthesis of graphene on copper with methanol, ethanol, and propanol precursors. *Carbon* **2011**, *49*, 4204–4210. [CrossRef]
52. Pu, J.; Wan, S.; Zhao, W.; Mo, Y.; Zhang, X.; Wang, L.; Xue, Q. Preparation and tribological study of functionalized graphene-IL nanocomposite ultrathin lubrication films on Si substrates. *J. Phys. Chem. C* **2011**, *115*, 13275–13284. [CrossRef]
53. Ullah, Z.; Riaz, S.; Li, Q.; Atiq, S.; Saleem, M.; Azhar, M.; Naseem, S.; Liu, L. A comparative study of graphene growth by APCVD, LPCVD and PECVD. *Mater. Res. Express* **2018**, *5*, 035606. [CrossRef]
54. Moharana, R.; Sengar, S.S.; Badhan, B.; Rao, U.S.; Gautam, R.K.; Tyagi, R. Tribological Behaviour of Graphene Coated Bearing Steel (EN31). *Phys. Conf. Ser.* **2019**, *1240*, 012040. [CrossRef]
55. Berman, D.; Erdemir, A.; Sumant, A. Reduced wear and friction enabled by graphene layers on sliding steel surfaces in dry nitrogen. *Carbon* **2013**, *59*, 167–175. [CrossRef]
56. *HertzWin, 3.3.1*; Vink System Design & Analysis: Eindhoven, The Netherlands, 2022.
57. Leach, R. *Characterisation of Areal Surface Texture*; Springer: Berlin/Heidelberg, Germany, 2013.
58. Waterworth, A. Quantitative Characterisation of Surface Finishes on Stainless Steel Sheet Using 3D Surface Topography Analysis. Ph.D. Thesis, University of Huddersfield, Huddersfield, UK, 2006.
59. Genta, G.; Maculotti, G. Uncertainty evaluation of small wear measurements on complex technological surfaces by machine vision-aided topographical methods. *CIRP Ann.* **2021**, *in press*. [CrossRef]
60. Maculotti, G.; Goti, E.; Genta, G.; Mazza, L.; Galetto, M. Uncertainty-based comparison of conventional and surface. *Tribol. Int.* **2022**, *165*, 107260. [CrossRef]
61. Nečas, D.; Klapetek, P. Gwyddion: An open-source software for SPM data analysis. *Cent. Eur. J. Phys.* **2012**, *10*, 181–188. [CrossRef]
62. Liang, H.; Bu, Y.; Zhang, J.; Cao, Z.; Liang, A. Graphene Oxide Film as Solid Lubricant. *ACS Appl. Mater. Interfaces* **2013**, *5*, 6369–6375. [CrossRef]
63. Long, F.; Yasaei, P.Y.W.; Salehi-Khojin, A.; Shahbazian-Yassar, R. Anisotropic Friction of Wrinkled Graphene Grown by Chemical Vapor Deposition. *ACS Appl. Mater. Interfaces* **2017**, *9*, 20922–20927. [CrossRef]
64. Paronyan, R.; Pigos, E.; Chen, G.; Harutyunyan, A.R. Formation of Ripples in Graphene as a result of Interfacial Instabilities. *ACS Nano* **2011**, *5*, 9619–9627. [CrossRef]
65. Comanescu, C. Single layer graphene Raman bands modifications as result of transfer from copper foil to oxidized silicon or quartz substrates. In Proceedings of the 2016 International Semiconductor Conference (CAS), Sinaia, Romania, 10–12 October 2016; pp. 49–52.
66. Huang, Z.; Chen, S.; Lin, Q.; Ji, Z.; Gong, P.; Sun, Z.; Shen, B. Microscopic Mechanisms Behind the High Friction and Failure. *Langmuir* **2021**, *37*, 6776–6782. [CrossRef]

67. Lee, C.; Li, Q.; Kalb, W.; Liu, X.-Z.; Berger, H.; Carpick, R.W.; Hone, J. Frictional Characteristics of Atomically Thin Sheets. *Science* **2010**, *328*, 76–80. [CrossRef] [PubMed]
68. Zeng, X.; Peng, Y.; Lang, H. A novel approach to decrease friction of graphene. *Carbon* **2017**, *118*, 233–240. [CrossRef]

Disclaimer/Publisher's Note: The statements, opinions and data contained in all publications are solely those of the individual author(s) and contributor(s) and not of MDPI and/or the editor(s). MDPI and/or the editor(s) disclaim responsibility for any injury to people or property resulting from any ideas, methods, instructions or products referred to in the content.